Proceedings of the 40th IEEE
Conference on Decision and Control
Orlando, Florida USA, December 2001

Stability of Hybrid System Limit Cycles: Application to the Compass Gait Biped Robot

Ian A. Hiskens[1]
Department of Electrical and Computer Engineering
University of Illinois at Urbana-Champaign
Urbana IL 61801 USA
hiskens@ece.uiuc.edu

Abstract

Limit cycles are common in hybrid systems. However the non-smooth dynamics of such systems makes stability analysis difficult. This paper uses recent extensions of trajectory sensitivity analysis to obtain the characteristic multipliers of non-smooth limit cycles. The stability of a limit cycle is determined by its characteristic multipliers. The concepts are illustrated using a compass gait biped robot example.

1 Introduction

Hybrid systems are characterized by interactions between continuous (smooth) dynamics and discrete events. Such systems are common across a diverse range of application areas. Examples include power systems [1], robotics [2, 3], manufacturing [4] and air-traffic control [5]. In fact, any system where saturation limits are routinely encountered can be thought of as a hybrid system. The limits introduce discrete events which (often) have a significant influence on overall behaviour.

Many hybrid systems exhibit periodic behaviour. Discrete events, such as saturation limits, can act to trap the evolving system state within a constrained region of state space. Therefore even when the underlying continuous dynamics are unstable, discrete events may induce a stable limit set. Limit cycles (periodic behaviour) are often created in this way. Other systems, such as robot motion, are naturally periodic. An example that builds on the analysis of a biped robot [3, 6] is presented in Section 5.

Limit cycles can be stable (attracting), unstable (repelling) or non-stable (saddle). The stability of periodic behaviour is determined by characteristic (or Floquet) multipliers. A periodic solution corresponds to a fixed point of a Poincaré map. Stability of the periodic solution is equivalent to stability of the fixed point. The characteristic multipliers are the eigenvalues of the Poincaré map linearized about the fixed point. Section 4 reviews the connection between this linearized map and trajectory sensitivities.

Poincaré maps have been used to analyse the stability of limit cycles in various forms of hybrid systems. However calculation of the underlying trajectory sensitivities has relied upon particular system structures, see for example [7, 8], or numerical differencing[1], for example [6]. This paper uses a recent generalization of trajectory sensitivity analysis [9] to efficiently determine the stability of limit cycles in hybrid systems.

A hybrid system model is given in Section 2. Section 3 develops the associated variational equations. This is followed in Section 4 by a review of stability analysis of limit cycles. An example is considered in Section 5. Conclusions and extensions are presented in Section 6.

2 Model

Deterministic hybrid systems can be represented by a model that is adapted from a differential-algebraic (DAE) structure. Events are incorporated via impulsive action and switching of algebraic equations, giving the *DA Impulsive Switched* (DAIS) model

$$\dot{x} = f(x,y) + \sum_{j=1}^{e} \delta(y_{e,j})\Big(h_j(x,y) - x\Big) \tag{1}$$

$$0 = g(x,y) \equiv g^{(0)}(x,y) + \sum_{i=1}^{d}\Big(g^{(i-)}(x,y) + u(y_{d,i})\Big(g^{(i+)}(x,y) - g^{(i-)}(x,y)\Big)\Big) \tag{2}$$

where

[1]Research supported by the EPRI/DoD Complex Interactive Networks/Systems Initiative, the National Science Foundation through grant ECS-0085755, and the Grainger Foundation.

[1]Each initial state of the system is perturbed. The difference between the perturbed and unperturbed trajectories is divided by the magnitude of the change in the initial state. This procedure is tedious, as it must be repeated for every state. It is also prone to numerical errors.

- $x \in \mathbb{R}^n$ are dynamic states and $y \in \mathbb{R}^m$ are algebraic states;
- $\delta(.)$ is the Dirac delta;
- $u(.)$ is the unit-step function;
- $f, h_j : \mathbb{R}^{n+m} \rightarrow \mathbb{R}^n$;
- $g^{(0)}, g^{(i\pm)} : \mathbb{R}^{n+m} \rightarrow \mathbb{R}^m$; some elements of each $g^{(.)}$ will usually be identically zero, but no elements of the composite g should be identically zero; the $g^{(i\pm)}$ are defined with the same form as g in (2), resulting in a recursive structure for g;
- y_d, y_e are selected elements of y that trigger algebraic switching and state reset (impulsive) events respectively; y_d and y_e may share common elements.

The impulse and unit-step terms of the DAIS model can be expressed in alternative forms:

- Each impulse term of the summation in (1) can be expressed in the state reset form

$$x^+ = h_j(x^-, y^-) \quad \text{when } y_{e,j} = 0 \tag{3}$$

  where the notation x^+ denotes the value of x just after the reset event, whilst x^- and y^- refer to the values of x and y just prior to the event.

- The contribution of each $g^{(i\pm)}$ in (2) can be expressed as

$$g^{(i)}(x,y) = \begin{cases} g^{(i-)}(x,y) & y_{d,i} < 0 \\ g^{(i+)}(x,y) & y_{d,i} > 0 \end{cases} \quad i = 1, ..., d$$

  with (2) becoming

$$0 = g(x,y) \equiv g^{(0)}(x,y) + \sum_{i=1}^{d} g^{(i)}(x,y). \tag{4}$$

  This form is often more intuitive than (2).

It can be convenient to establish the partitions

$$x = \begin{bmatrix} \underline{x} \\ z \\ \lambda \end{bmatrix}, \qquad f = \begin{bmatrix} \underline{f} \\ 0 \\ 0 \end{bmatrix}, \qquad h_j = \begin{bmatrix} \underline{x} \\ \underline{h}_j \\ \lambda \end{bmatrix} \tag{5}$$

where

- $\underline{x}$ are the continuous dynamic states, for example generator angles, velocities and fluxes;
- z are discrete dynamic states, such as transformer tap positions and protection relay logic states;
- λ are parameters such as generator reactances, controller gains and switching times.

The partitioning of the differential equations f ensures that away from events, $\underline{x}$ evolves according to $\dot{\underline{x}} = \underline{f}(x,y)$, whilst z and λ remain constant. Similarly, the partitioning of the reset equations h_j ensures that $\underline{x}$ and λ remain constant at reset events, but the dynamic states z are reset to new values given by $z^+ = \underline{h}_j(x^-, y^-)$.

The model can capture complex behaviour, from hysteresis and non-windup limits through to rule-based systems [1]. A more extensive presentation of this model is given in [9].

Away from events, system dynamics evolve smoothly according to the familiar differential-algebraic model

$$\dot{x} = f(x,y) \tag{6}$$
$$0 = g(x,y) \tag{7}$$

where g is composed of $g^{(0)}$ together with appropriate choices of $g^{(i-)}$ or $g^{(i+)}$, depending on the signs of the corresponding elements of y_d. At switching events (2), some component equations of g change. To satisfy the new $g = 0$ equation, algebraic variables y may undergo a step change. Reset events (3) force a discrete change in elements of x. Algebraic variables may also step at a reset event to ensure $g = 0$ is satisfied with the altered values of x.

The *flows* of x and y are defined respectively as

$$x(t) = \phi_x(x_0, t) \tag{8}$$
$$y(t) = \phi_y(x_0, t) \tag{9}$$

where $x(t)$ and $y(t)$ satisfy (1),(2), along with initial conditions,

$$\phi_x(x_0, t_0) = x_0 \tag{10}$$
$$g(x_0, \phi_y(x_0, t_0)) = 0. \tag{11}$$

3 Trajectory Sensitivities

Sensitivity of the flows ϕ_x and ϕ_y to initial conditions x_0 are obtained by linearizing (8),(9) about the nominal trajectory,

$$\Delta x(t) = \frac{\partial \phi_x(x_0, t)}{\partial x_0} \Delta x_0 \tag{12}$$
$$\Delta y(t) = \frac{\partial \phi_y(x_0, t)}{\partial x_0} \Delta x_0. \tag{13}$$

The time-varying partial derivative matrices given in (12),(13) are known as *trajectory sensitivities*, and can be expressed in the alternative forms

$$\frac{\partial \phi_x(x_0, t)}{\partial x_0} \equiv x_{x_0}(t) \equiv \Phi_x(x_0, t) \tag{14}$$
$$\frac{\partial \phi_y(x_0, t)}{\partial x_0} \equiv y_{x_0}(t) \equiv \Phi_y(x_0, t). \tag{15}$$

The form x_{x_0}, y_{x_0} provides clearer insights into the development of the variational equations describing the evolution of the sensitivities. The alternative form $\Phi_x(x_0,t)$, $\Phi_y(x_0,t)$ highlights the connection between the sensitivities and the associated flows. It is shown in Section 4 that these sensitivities underlie the linearization of the Poincaré map, and so play a major role in determining the stability of periodic solutions.

Away from events, where system dynamics evolve smoothly, trajectory sensitivities x_{x_0} and y_{x_0} are obtained by differentiating (6),(7) with respect to x_0. This gives

$$\begin{aligned} \dot{x}_{x_0} &= f_x(t)x_{x_0} + f_y(t)y_{x_0} && (16)\\ 0 &= g_x(t)x_{x_0} + g_y(t)y_{x_0} && (17)\end{aligned}$$

where $f_x \equiv \partial f/\partial x$, and likewise for the other Jacobian matrices. Note that f_x, f_y, g_x, g_y are evaluated along the trajectory, and hence are time varying matrices. It is shown in [9, 10] that the numerical solution of this (potentially high order) DAE system can be obtained as a by-product of numerically integrating the original DAE system (6),(7). The extra computational cost is minimal.

Initial conditions for x_{x_0} are obtained from (10) as

$$x_{x_0}(t_0) = I$$

where I is the identity matrix. Initial conditions for y_{x_0} follow directly from (17),

$$0 = g_x(t_0) + g_y(t_0)y_{x_0}(t_0).$$

Equations (16),(17) describe the evolution of the sensitivities x_{x_0} and y_{x_0} between events. However at an event, the sensitivities are generally discontinuous. It is necessary to calculate *jump conditions* describing the step change in x_{x_0} and y_{x_0}. For clarity, consider a single switching/reset event, so the model (1),(2) reduces (effectively) to the form

$$\dot{x} = f(x,y) \qquad (18)$$

$$0 = \begin{cases} g^-(x,y) & s(x,y) < 0 \\ g^+(x,y) & s(x,y) > 0 \end{cases} \qquad (19)$$

$$x^+ = h(x^-,y^-) \qquad s(x,y) = 0. \qquad (20)$$

Let $(x(\tau), y(\tau))$ be the point where the trajectory encounters the triggering hypersurface $s(x,y) = 0$, i.e., the point where an event is initiated. This point is called the *junction point* and τ is the *junction time*. It is assumed the encounter is transversal.

Just prior to event triggering, at time τ^-, we have

$$\begin{aligned} x^- = x(\tau^-) &= \phi_x(x_0,\tau^-) \\ y^- = y^-(\tau^-) &= \phi_y(x_0,\tau^-) \end{aligned}$$

where

$$g^-(x^-,y^-) = 0.$$

Similarly, x^+, y^+ are defined for time τ^+, just after the event has occurred. It is shown in [9] that the jump conditions for the sensitivities x_{x_0} are given by

$$x_{x_0}(\tau^+) = h_x^*\, x_{x_0}(\tau^-) - \left(f^+ - h_x^*\, f^-\right)\tau_{x_0} \qquad (21)$$

where

$$\begin{aligned} h_x^* &= \left(h_x - h_y(g_y^-)^{-1}g_x^-\right)\big|_{\tau^-} \\ \tau_{x_0} &= -\frac{\left(s_x - s_y(g_y^-)^{-1}g_x^-\right)\big|_{\tau^-} x_{x_0}(\tau^-)}{\left(s_x - s_y(g_y^-)^{-1}g_x^-\right)\big|_{\tau^-} f^-} \\ f^- &= f(x(\tau^-), y^-(\tau^-)) \\ f^+ &= f(x(\tau^+), y^+(\tau^+)). \end{aligned}$$

The assumption that the trajectory and triggering hypersurface meet transversally ensures a non-zero denominator for τ_{x_0}. The sensitivities y_{x_0} immediately after the event are given by

$$y_{x_0}(\tau^+) = -\left(g_y^+(\tau^+)\right)^{-1} g_x^+(\tau^+)x_{x_0}(\tau^+).$$

Following the event, i.e., for $t > \tau^+$, calculation of the sensitivities proceeds according to (16),(17) until the next event is encountered. The jump conditions provide the initial conditions for the post-event calculations.

4 Limit Cycle Analysis

Stability of limit cycles can be determined using Poincaré maps [11, 12]. This section provides a brief review of these concepts, and establishes the connection with trajectory sensitivities.

A Poincaré map effectively samples the flow of a periodic system once every period. The concept is illustrated in Figure 1. If the limit cycle is stable, oscillations approach the limit cycle over time. The samples provided by the corresponding Poincaré map approach a fixed point. A non-stable limit cycle results in divergent oscillations. For such a case the samples of the Poincaré map diverge.

To define a Poincaré map, consider the limit cycle Γ shown in Figure 1. Let Σ be a hyperplane transversal to Γ at x^*.[2] The trajectory emanating from x^* will again encounter Σ at x^* after T seconds, where T is the minimum period of the limit cycle. Due to the continuity of the flow ϕ_x with respect to initial conditions, trajectories starting on Σ in a neighbourhood of x^* will, in approximately T seconds, intersect Σ in the vicinity of x^*. Hence ϕ_x and Σ define a mapping

$$x_{k+1} = P(x_k) := \phi_x(x_k, \tau_r(x_k)). \qquad (22)$$

[2]The fixed point x^* can be located using shooting methods [12], even for hybrid systems. Trajectory sensitivities provide the gradient information required by these Newton-based methods.

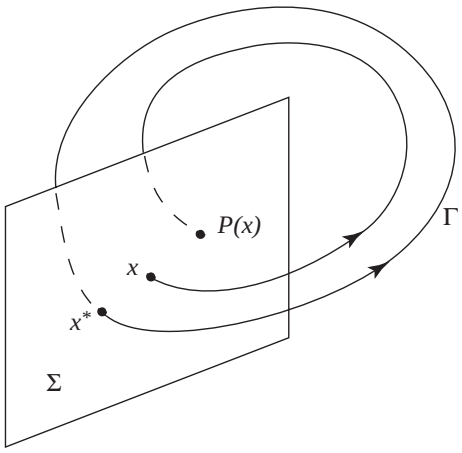

Figure 1: Poincaré map.

where $\tau_r(x_k) \approx T$ is the time taken for the trajectory to return to Σ. Complete details can be found in [11, 12].

Stability of the Poincaré map (22) is determined by linearizing P at the fixed point x^*, i.e.,

$$\Delta x_{k+1} = DP(x^*)\Delta x_k. \tag{23}$$

From the definition of $P(x)$ given by (22), it follows that $DP(x^*)$ is closely related to the trajectory sensitivities $\frac{\partial \phi_x(x^*,T)}{\partial x^*} \equiv \Phi_x(x^*,T)$. In fact, it is shown in [11] that

$$DP(x^*) = \left(I - \frac{f(x^*,y^*)\sigma^t}{f(x^*,y^*)^t\sigma}\right)\Phi_x(x^*,T) \tag{24}$$

where σ is a vector normal to Σ.

The matrix $\Phi_x(x^*,T)$ is exactly the trajectory sensitivity matrix after one period of the limit cycle, i.e., starting from x^* and returning to x^*. This matrix is called the *Monodromy matrix*. It is shown in [11] that for an autonomous system, one eigenvalue of $\Phi_x(x^*,T)$ is always 1, and the corresponding eigenvector lies along $f(x^*,y^*)$. The remaining eigenvalues of $\Phi_x(x^*,T)$ coincide with the eigenvalues of $DP(x^*)$, and are known as the *characteristic multipliers* m_i of the periodic solution. The characteristic multipliers are independent of the choice of cross-section Σ. Therefore, for hybrid systems, it is often convenient to choose Σ as a triggering hypersurface corresponding to a switching or reset event that occurs along the periodic solution.

Because the characteristic multipliers m_i are the eigenvalues of the linear map $DP(x^*)$, they determine the stability of the Poincaré map $P(x_k)$, and hence the stability of the periodic solution. Three cases are of importance:

1. All m_i lie within the unit circle, i.e., $|m_i| < 1, \forall i$. The map is stable, so the periodic solution is stable.
2. All m_i lie outside the unit circle. The periodic solution is unstable.
3. Some m_i lie outside the unit circle. The periodic solution is non-stable.

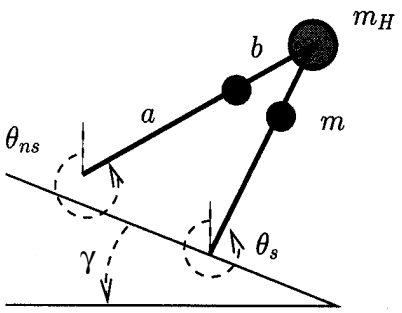

Figure 2: Compass gait biped robot.

Interestingly, there exists a particular cross-section Σ^*, such that

$$DP(x^*)\zeta = \Phi_x(x^*,T)\zeta \tag{25}$$

where $\zeta \in \Sigma^*$. This cross-section Σ^* is the hyperplane spanned by the $n-1$ eigenvectors of $\Phi_x(x^*,T)$ that are not aligned with $f(x^*,y^*)$. Therefore the vector σ^* that is normal to Σ^* is the left eigenvector of $\Phi_x(x^*,T)$ corresponding to the eigenvalue 1. The hyperplane Σ^* is invariant under $\Phi_x(x^*,T)$, i.e., $\Phi_x(x^*,T)$ maps vectors $\zeta \in \Sigma^*$ back into Σ^*.

5 Example

5.1 Model

A model of the compass gait biped robot is discussed in detail in [3, 6]. A summary is included here for completeness. The biped robot can be treated as a double pendulum, with point masses m_H and m concentrated at the hips and legs respectively. Figure 2 provides a schematic representation and identifies other important parameters, lengths a and b, and incline angle γ. The robot configuration is described by the *support angle* θ_s and the *non-support angle* θ_{ns}. The dynamic equations describing the robot can be written

$$M(\theta)\ddot{\theta} + N(\theta,\dot{\theta})\dot{\theta} + \frac{1}{a}g(\theta) = 0 \tag{26}$$

where $\theta = [\theta_{ns}\ \theta_s]^t$. The state vector is therefore $x = [\theta_{ns}\ \theta_s\ \dot{\theta}_{ns}\ \dot{\theta}_s]^t \in \mathbb{R}^4$. The matrices of (26) are given by,

$$M(\theta) = \begin{bmatrix} \beta^2 & -(1+\beta)\beta\cos\theta_d \\ -(1+\beta)\beta\cos\theta_d & (1+\beta)^2(\mu+1)+1 \end{bmatrix}$$

$$N(\theta,\dot{\theta}) = \begin{bmatrix} 0 & (1+\beta)\beta\dot{\theta}_s\sin\theta_d \\ -(1+\beta)\beta\dot{\theta}_{ns}\sin\theta_d & 0 \end{bmatrix}$$

$$g(\theta) = \begin{bmatrix} g\beta\sin\theta_{ns} \\ -((\mu+1)(1+\beta)+1)g\sin\theta_s \end{bmatrix}$$

where $\theta_d = \theta_s - \theta_{ns}$, $\beta = b/a$, $\mu = m_H/m$, and $g = 9.8$ is the gravitational constant. The model can be simply manipulated into the form (1), though the impulse effects are added below.

An event occurs when the non-support (swinging) leg collides with the ground. This establishes the triggering condition

$$\theta_{ns} + \theta_s + 2\gamma = 0. \tag{27}$$

At the event, the non-support leg becomes the support leg, and vice-versa. Velocities $\dot{\theta}_{ns}$ and $\dot{\theta}_s$ undergo step changes to ensure conservation of momentum through the collision. The resulting reset equations can be written

$$\begin{bmatrix} \theta \\ \dot{\theta} \end{bmatrix}^+ = \begin{bmatrix} \begin{bmatrix} 0 & 1 \\ 1 & 0 \end{bmatrix} & 0 \\ 0 & Q^+(\theta_d^-)^{-1}Q^-(\theta_d^-) \end{bmatrix} \begin{bmatrix} \theta \\ \dot{\theta} \end{bmatrix}^- \tag{28}$$

where

$$Q^+(\theta_d) = \begin{bmatrix} \beta\big(\beta - (1+\beta)\cos\theta_d\big) & (1+\beta)\big((1+\beta) - \beta\cos\theta_d\big) \\ & \ldots + 1 + \mu(1+\beta)^2 \\ \beta^2 & -\beta(1+\beta)\cos\theta_d \end{bmatrix}$$

$$Q^-(\theta_d) = \begin{bmatrix} -\beta & -\beta + \big(\mu(1+\beta)^2 + 2(1+\beta)\big)\cos\theta_d \\ 0 & -\beta \end{bmatrix}.$$

Equation (28) matches the form (3). The event triggering state y_e follows from (27) as $y_e = \theta_{ns} + \theta_s + 2\gamma$.

5.2 Results

Parameter values of $\beta = 1$, $\mu = 2$, $a = 0.5$ and $\gamma = 3^o$ were used for the base case. Two views of the corresponding limit cycle are shown in Figure 3. The left figure shows the limit cycle in terms of states θ_{ns}, θ_s, $\dot{\theta}_{ns}$ and $\dot{\theta}_s$. The right view shows the behaviour of each leg through a full cycle. Recall that each leg acts as the support leg for half the cycle, and the non-support leg for the other half cycle. Therefore a complete walking cycle (right view) is formed from the limit cycle of the states (left view). It follows that the period of the walking cycle is twice the period of the state limit cycle.

The triggering hypersurface corresponding to the ground collision provides a convenient cross-section Σ for defining a Poincaré map. Consider the point $x^* = [0.2188 \quad -0.3236 \quad -1.8056 \quad -1.4939]^t$ on the limit cycle immediately prior to the switching event. Based on this choice for x^*, the eigenvalues of the trajectory sensitivity matrix $\Phi_x(x^*, T)$ after one period of the limit cycle are

$$0.9992, \quad -0.2035 \pm j0.5430, \quad 0.1315. \tag{29}$$

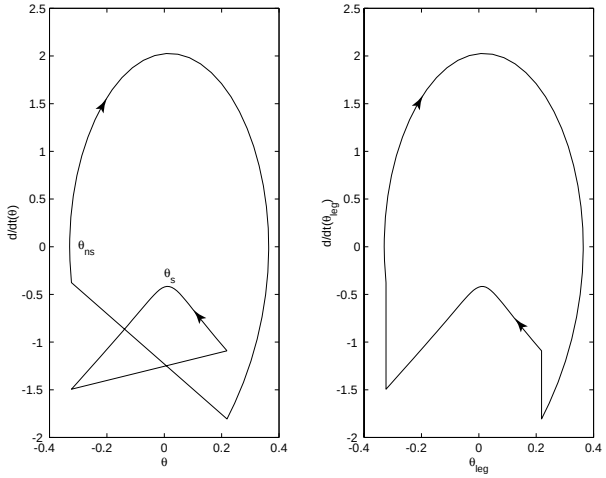

Figure 3: Base case limit cycle.

The eigenvector corresponding to the (near) unity eigenvalue is

$$\begin{aligned} ev_1 &= [0.1518 \; 0.1256 \; 0.8856 \; 0.4206]^t \\ &= -0.0842 f(x^*, y^*). \end{aligned}$$

Therefore, as anticipated, the eigenvector corresponding to the unity eigenvalue is aligned with $f(x^*, y^*)$. The other eigenvalues are the characteristic multipliers for this limit cycle. Their magnitudes are less than one, confirming that the limit cycle is stable. These results are in agreement with the characteristic multipliers obtained in [6]. Note though that the multipliers in [6] correspond to a walking cycle, which consists of two cycles of the states. In that case the multipliers are the eigenvalues of $\Phi_x(x^*, 2T) = \Phi_x(x^*, T)^2$, i.e., the eigenvalues are the square of the values given in (29).

As the angle of incline γ increases, robot behaviour undergoes a sequence of period doubling bifurcations [3]. Efficient computation of trajectory sensitivities, as proposed in Section 3, makes it feasible to track characteristic multipliers through these bifurcations. Figure 4 shows the locus of the multipliers as the first bifurcation is approached. Beginning from $\gamma = 3^o$, the complex multipliers merge at $\gamma = 4.07^o$, then split along the real axis. The bifurcation occurs at an incline angle of $\gamma = 4.37^o$, at which point one of the multipliers equals -1. Beyond that critical parameter value, the single-period limit cycle becomes unstable, with behaviour repeating every two cycles.

Figure 5 shows behaviour for an incline of $\gamma = 4.4^o$, i.e., just beyond the period-doubling bifurcation. The double period is evident in the state trajectories in the left figure. The corresponding view of leg behaviour is shown in the right view. Each leg now follows a (slightly) different trajectory, i.e., the robot limps!

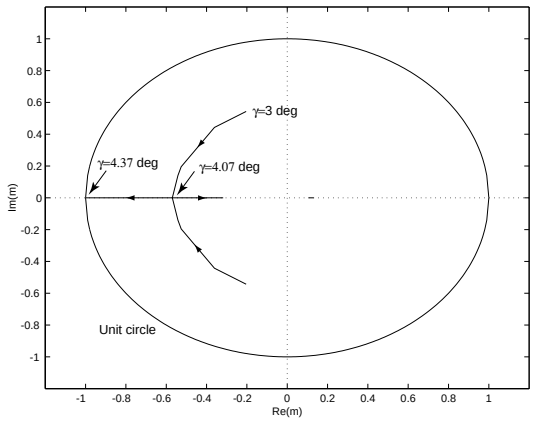

Figure 4: Locus of multipliers as incline increased.

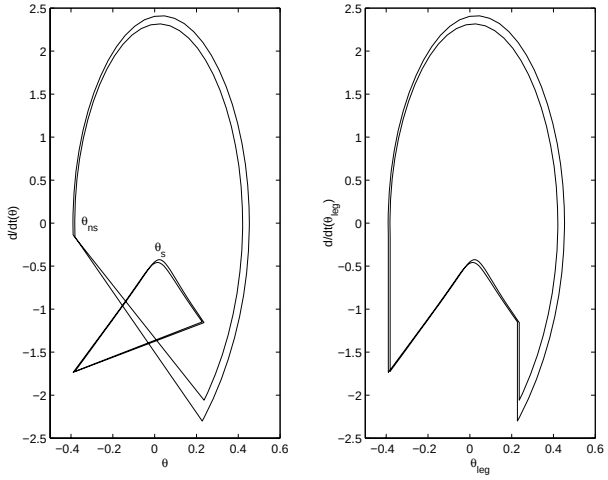

Figure 5: Double period limit cycle.

6 Conclusions

Hybrid systems frequently exhibit periodic behaviour. However the non-smooth nature of such systems complicates stability analysis. Those complications have been addressed in this paper through application of a generalization of trajectory sensitivity analysis.

Deterministic hybrid systems can be represented by a set of differential-algebraic equations, modified to incorporate impulse (state reset) action and constraint switching. The associated variational equations establish jump conditions that describe the evolution of sensitivities through events. These equations provide insights into expansion/contraction effects at events. This is a focus of future research.

Standard Poincaré map results extend naturally to hybrid systems. The Monodromy matrix is obtained by evaluating trajectory sensitivities over one period of the (possibly non-smooth) cyclical behaviour. One eigenvalue of this matrix is always unity. The remaining eigenvalues are the characteristic multipliers of the periodic solution. Stability is ensured if all multipliers lie inside the unit circle. Instability occurs if any multiplier lies outside the unit circle.

References

[1] I.A. Hiskens and M.A. Pai, "Hybrid systems view of power system modelling," in *Proceedings of the IEEE International Symposium on Circuits and Systems*, Geneva, Switzerland, May 2000.

[2] M.H. Raibert, *Legged Robots That Balance*, MIT Press, Cambridge, MA, 1986.

[3] A. Goswami, B. Thuilot, and B. Espiau, "A study of the passive gait of a compass-like biped robot: symmetry and chaos," *International Journal of Robotics Research*, vol. 17, no. 15, 1998.

[4] S. Pettersson, "Analysis and design of hybrid systems," Ph.D. Thesis, Department of Signals and Systems, Chalmers University of Technology, Göteborg, Sweden, 1999.

[5] C. Tomlin, G. Pappas, and S. Sastry, "Conflict resolution for air traffic management: A study in multiagent hybrid systems," *IEEE Transactions on Automatic Control*, vol. 43, no. 4, pp. 509–521, April 1998.

[6] A. Goswami, B. Espiau, and A. Keramane, "Limit cycles in a passive compass gait biped and passivity-mimicking control laws," *Journal of Autonomous Robots*, vol. 4, no. 3, 1997.

[7] B.K.H. Wong, H.S.H. Chung, and S.T.S. Lee, "Computation of the cycle state-variable sensitivity matrix of PWM DC/DC converters and its application," *IEEE Transactions on Circuits and Systems I*, vol. 47, no. 10, pp. 1542–1548, October 2000.

[8] M. Rubensson, B. Lennartsson, and S. Pettersson, "Convergence to limit cycles in hybrid systems - an example," in *Preprints of 8th International Federation of Automatic Control Symposium on Large Scale Systems: Theory & Applications*, Rio Patras, Greece, 1998, pp. 704–709.

[9] I.A. Hiskens and M.A. Pai, "Trajectory sensitivity analysis of hybrid systems," *IEEE Transactions on Circuits and Systems I*, vol. 47, no. 2, pp. 204–220, February 2000.

[10] D. Chaniotis, M.A. Pai, and I.A. Hiskens, "Sensitivity analysis of differential-algebraic systems using the GMRES method - Application to power systems," in *Proceedings of the IEEE International Symposium on Circuits and Systems*, Sydney, Australia, May 2001.

[11] T.S Parker and L.O. Chua, *Practical Numerical Algorithms for Chaotic Systems*, Springer-Verlag, New York, NY, 1989.

[12] R. Seydel, *Practical Bifurcation and Stability Analysis*, Springer-Verlag, New York, 2nd edition, 1994.